CrystEngComm

Cite this: *CrystEngComm*, 2011, **13**, 7262

www.rsc.org/crystengcomm

PAPER

Synthesis and formation mechanism of helical single-crystalline $CuInSe_2$ nanowires

Liang Shi*[a] and Quan Li[b]

Received 23rd June 2011, Accepted 1st September 2011
DOI: 10.1039/c1ce05777d

Highly ordered single-crystalline $CuInSe_2$ nanowires array have been prepared *via* a facile solution approach by using anodic aluminium oxide (AAO) as a hard template. $CuInSe_2$ nanowires with a novel helical shape are found to be formed by this approach. A screw-dislocation-induced growth process is proposed for the formation mechanism of this interesting nanostructure based on detailed structural characterizations. The $CuInSe_2$ helical nanowires have an average diameter of 200 nm and a periodicity of about 50–100 nm. Another type of $CuInSe_2$ nanowire with a straight shape is also found in the product and an oriented attachment mechanism has been used to explain its growth. Nanowires with both types of shapes have the same [112] growth direction. The structure, morphology, composition and optical absorption properties of the as-prepared samples were characterized using X-ray powder diffraction, transmission electron microscopy, energy dispersive X-ray spectrometry, scanning electron microscopy and UV-Vis spectrophotometry.

1. Introduction

Copper indium diselenide ($CuInSe_2$) is an important ternary I–III–VI_2 chalcopyrite semiconductor. It has triggered intense interests of researchers recently due to its unique structural and superior electrical properties.[1,2] For example, $CuInSe_2$ has good radiation stability, high optical absorption coefficient ($\sim 10^5$/cm) and a direct band-gap with a band energy ($\sim$1.05 eV) at the red edge of the solar spectrum,[3,4] which make this material an ideal candidate for the production of photochemical devices. Solar cells based on this material have achieved a power conversion efficiency of nearly 20%.[5] Up to now, $CuInSe_2$ nanostructures have been prepared successfully by various methods,[6–8] aiming at employing these nanoparticles for high performance photovoltaic devices by adopting the ink printing technology because it is expected that nanoscale I–III–VI_2 materials provide a potential for multiexciton-generation-enhanced efficiencies.[9] Nevertheless, the preparation of single crystalline $CuInSe_2$ nanowires in a well-aligned array configuration has not yet been studied extensively.[10,11] Semiconductors in the nanowire morphology can offer a well-defined nanoscale domain with clearly identifiable grain boundaries, where an energy barrier exists and prevents charge carrier recombination,[12,13] being beneficial to the conversion efficiency improvement. In addition, the well-aligned $CuInSe_2$ nanowires may provide continuous charge carrier transport pathways without dead ends. As a result, further increase in conversion efficiency might be expected in the nanowire photovoltaic devices.[14] The template method assisted by porous anodic aluminium oxide (AAO) is one of the most efficient methods for the fabrication of highly ordered well-distributed one-dimensional nanostructures, especially for polynary compound nanowires.[15–17] AAO has many advantages including monodisperse size distribution, high pore density, nearly parallel porous structures and easily controlled pore diameter.[18,19] Furthermore, the AAO template can be employed in rigorous reaction conditions that arise from its thermal and mechanical stability.

Here we report a facile solution approach with AAO as a hard template for preparation of an array of well-aligned uniform single crystalline $CuInSe_2$ nanowires. Two types of shape of $CuInSe_2$ nanowires were found to co-exist in the sample: one is straight nanowires, the other one is novel helical nanowires. Elaboration on the formation mechanisms of the two types of shapes of $CuInSe_2$ nanowires is conducted respectively.

2. Experimental section

All reagents are of analytical grade and used without further purification. Anhydrous oleylamine (OLA), CuCl, anhydrous $InCl_3$, and elemental selenium were used as starting materials. AAO templates (Whatman Co., UK) with pore sizes of 200 nm in diameter were used in the experiments. In a typical procedure, for the fabrication of the $CuInSe_2$ nanowires array within the AAO template, 1 mmol of CuCl (0.099 g), 1 mmol of $InCl_3$ (0.221 g), and 2 mmol of elemental Se (0.158 g) were added to a 25 mL three-neck flask in air. Then 20 mL OLA were added into the above flask with mild magnetic stirring. Afterward, an AAO template was added into the flask and immersed in the liquid.

[a]*Department of Chemistry, University of Science and Technology of China, Hefei, 230026, P. R. China. E-mail: sliang@ustc.edu.cn; Fax: +86-551-3607402; Tel: +86-551-3607234*
[b]*Department of Physics, The Chinese University of Hong Kong, Shatin, New Territory, Hong Kong, P. R. China*

The above liquid mixture in the flask was treated by sonication for 10 min to remove air in the pores of the AAO template and fill the pores with liquid. The flask was attached to a Schlenk line and purged of oxygen and water by pulling vacuum for 30 min, followed by nitrogen bubbling for 30 min with mild magnetic stirring. The evacuation and N_2 bubbling processes were cycled for 3 times at room temperature. The flask was then heated to 110 °C whilst maintaining a N_2 flow. The evacuation and nitrogen bubbling processes were conducted at 110 °C again once. The sonication and multi-evacuation and bubbling process was important to enhance the filling efficiency of the AAO template pores with the mixture of reaction solution. The mixture is then heated to 210 °C, and the reaction proceeds for 2 h under N_2 flow with vigorous stirring. The reaction was allowed to cool to room temperature and the AAO template containing the product was taken out from the flask, thoroughly washed with ethanol and distilled water, and then dried in air.

The overall crystallinity of the product is examined by X-ray diffraction (XRD, Rigakau RU-300 with Cu-Kα radiation). Room-temperature Raman spectra were measured using a micro-laser Raman spectrometer (Renishaw) in a back-scattering configuration, employing the 514.5 nm line of an Ar laser as the excitation source. The general morphology of the products was characterized using scanning electron microscopy (FESEM QF400). Detailed microstructure analysis was carried out using transmission electron microscopy (TEM Tecnai 20ST). Chemical composition analysis was obtained by energy dispersive X-ray spectrometry (EDX) using an EDX spectrometer attached to the same microscope. For the SEM measurements, several drops of 1 M NaOH aqueous solution were added onto the sample to dissolve some part of the AAO template. The residual solution on the surface of the template was rinsed with distilled water. For the TEM and HRTEM measurements, the template was completely dissolved in 2 M NaOH aqueous solution. The product was centrifuged, thoroughly washed with distilled water to remove residual NaOH and then rinsed with absolute ethanol.

3. Results and discussion

Fig. 1 shows typical SEM images of the as-prepared $CuInSe_2$ product with the AAO template partially removed. The top view of the sample in Fig. 1a indicates that an array made up of large-area dense nanowires with uniform diameter is formed. The side view image in Fig. 1b discloses clearly that these nanowires are smooth and of several micrometres in length. These nanowires are also found to be compact and parallel to each other, maintaining a nanowire array structure from the side view.

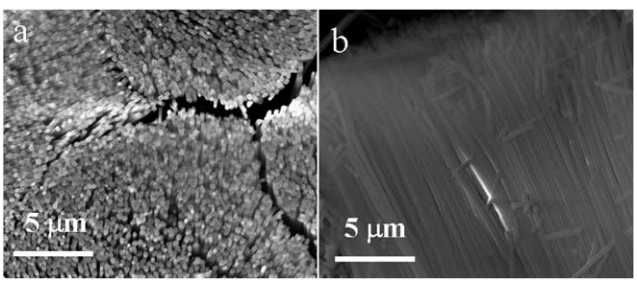

Fig. 1 (a) Top view and (b) side view SEM images of the as-prepared $CuInSe_2$ nanowires array.

The crystal structure of the product was firstly characterized by X-ray diffraction (XRD). A typical XRD pattern of the as-prepared $CuInSe_2$ product embedded in AAO pores is shown in Fig. 2. All diffraction peaks can be indexed to the tetragonal chalcopyrite structured $CuInSe_2$. After refinement, the lattice constants, $a = 5.780$ Å and $c = 11.617$ Å, are obtained, which match well to the reported values for the $CuInSe_2$ crystal (JCPDS card, No. 40-1487). The broadening of the XRD peaks suggests that the grain sizes of the product are on a nanometre scale. No signals of impurities or side products were found in the product. An increasing background at small diffraction angles can be found in the XRD pattern, which is induced by diffraction of the amorphous AAO hard template.

Raman scattering spectroscopy was employed to investigate the crystal quality and vibration properties of the as-prepared $CuInSe_2$ nanostructures. Fig. 3 shows a typical room-temperature Raman spectrum for the $CuInSe_2$ product in the range of 100–500 cm^{-1}. It can be observed that a much strong peak at 175 cm^{-1} and a very weak peak at about 212 cm^{-1}, similar to the Raman spectrum of $CuInSe_2$ films where the 750 cm^{-1} peak is much stronger than any other ones. In the tetragonal CuInSe2 crystal, the 750 cm^{-1} peak is reported to originate from the A1 optical phonon mode,[20] which has the largest Raman cross-section and is induced by the vibration of two pairs of anions, one in the direction of the *a*-axis and the other in the direction of the *b*-axis.[21] The sharp peak of the A1 optical phonon mode suggests the better crystallization of the $CuInSe_2$ nanostructure and uniform particle size; this is in good agreement with the above SEM and XRD results.

The $CuInSe_2$ sample was observed to be black due to the strong photon absorption in the entire visible range of light, suggesting their potential in solar energy conversation applications. Fig. 4 shows the room temperature UV-Vis absorption spectrum for the as prepared $CuInSe_2$ nanowires sample. Estimation on the optical band gap (E_g) of the $CuInSe_2$ nanowires can be obtained by plotting $(\alpha h\nu)^2$ as a function of the photon energy (in the inset of Fig. 4), with α being the absorption coefficient, h Planck's constant, and ν the frequency. The E_g value is estimated as 1.04 eV from the intersection of the

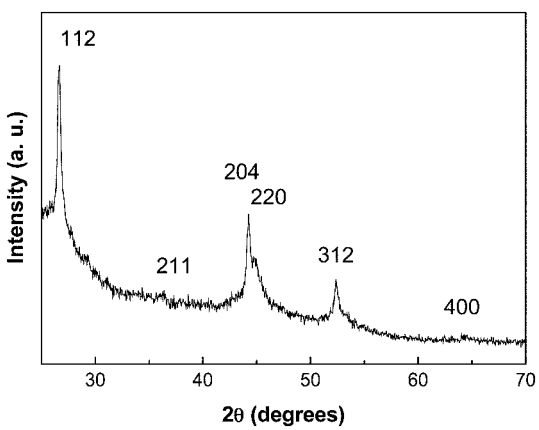

Fig. 2 Representative XRD patterns of the as-prepared $CuInSe_2$ nanowires array.

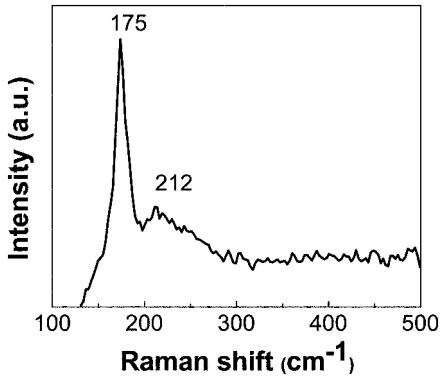

Fig. 3 Room-temperature Raman spectrum of the as-prepared $CuInSe_2$ nanowires.

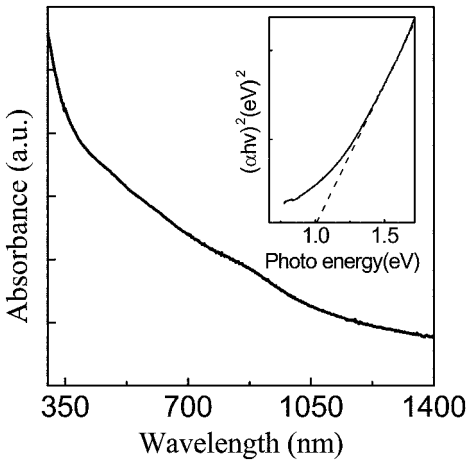

Fig. 4 A typical room-temperature UV-Vis absorbance spectrum of the as-prepared $CuInSe_2$ nanowires.

extrapolated linear portion with the *x*-axis (photon energy), being consistent with the reported values of $CuInSe_2$ in literature.[22,23] Such a band gap value is desirable for the photovoltaic and photocatalytic applications.

TEM studies accompanied by selected area electron diffraction (SAED) and energy dispersive X-ray spectrometry (EDX) were performed to characterize the morphology, structures and chemical composition of the $CuInSe_2$ nanowires. Under TEM observation, two types of shapes of $CuInSe_2$ nanowires were found to co-exist in the sample: one is straight nanowires, the other one is helical nanowires. A typical TEM image of the straight nanowires in Fig. 5a discloses that the $CuInSe_2$ nanowires are straight with a smooth surface. $CuInSe_2$ nanowires are all found to have an average diameter of about 200 nm, which is consistent with the pore size dimension of the AAO template. The EDX spectrum (Fig. 5b) taken from the sample shows intense peaks of Cu, In and Se, suggesting the composition of Cu, In and Se, only. The gold and carbon signals come from the supporting TEM grid. EDX quantitative analysis gives an average Cu/In/Se composition ratio of 1 : 1 : 2, in accordance with the stoichiometry of $CuInSe_2$. EDX elemental maps (as shown in Fig. 5e–h) of Cu, In, and Se give information on the spatial distribution of the compositional elements. The uniform spatial distribution of the different compositional elements is clarified evident in the elemental maps. A high resolution TEM (HRTEM) image shown in Fig. 5c shows a clear lattice spacing of 0.335 nm which is calculated from the line profile in Fig. 5d. This corresponds well to the *d* spacing of the (112) planes in the tetragonal chalcopyrite structured $CuInSe_2$, confirming the well-crystallized single crystals of the $CuInSe_2$ nanowires. The HRTEM analysis displays that the $CuInSe_2$ nanowires grow along the [112] direction. The inset of Fig. 5c shows a two-dimensional Fourier transform pattern of the lattice resolved image, which can be indexed to the $[1\bar{1}0]$ zone of hexagonal $CuInSe_2$, demonstrating further the [112] growth direction and single crystallinity of the $CuInSe_2$ nanowires.

The TEM images of helical $CuInSe_2$ nanowires are shown in Fig. 6. Fig. 6a indicates the helical shape of the nanowire with a diameter of about 200 nm. A typical SEM image of a $CuInSe_2$ helical nanowire is shown in lower left inset of Fig. 6a. The upper right inset of Fig. 6a is a selected area electron diffraction pattern of the helical $CuInSe_2$ nanowires with clear diffraction spots, confirming the single crystalline nature of the helical $CuInSe_2$ nanowires. Out-of-focus diffraction indicates that the nanowires grow along the [112] direction. It is also found that the helical $CuInSe_2$ nanowires have a periodicity of about 50–100 nm. Obtained from part of the nanowire (as shown as a white square) in Fig. 6a, an HRTEM image of the helical $CuInSe_2$ nanowires in Fig. 6b displays a clear lattice image, confirming further that the helical $CuInSe_2$ nanowires are highly crystalline. HRTEM observation also displays that some dislocation exists in the helical nanowires, as shown with arrows in Fig. 6c. Fig. 6d displays that the bottom of the helical nanowire has a cone shaped hollow. Actually, the cone shaped protrusion in the tip of the helical nanowires is also observed. A broken part of the helical nanowire in Fig. 6e shows both the cone shape of the concave bottom and the protrusion tip with almost the same cone angle, suggesting that the nanowires snap at the same growth facets. The helical shape of the nanowires and the cone shape of the concave bottom and protrusion tip disclose that the formation mechanism of this kind of helical structured nanowires may be by screw-dislocation-induced growth. We will discuss this in detail later.

The discussion on the possible formation mechanism of the $CuInSe_2$ and nanowires array could be proposed as follows based on our experimental results. Chemically, the choice of oleylamine as solvent is critical for the synthesis of $CuInSe_2$. As an organic base, oleylamine provided a stronger reductive environment and can decrease the precursor decomposition temperature dramatically.[24] In the present reaction process, oleylamine acted as an activation agent, expediting the precursor decomposition process at low temperature. As a result, the reactivity difference of the precursors is almost removed, which facilitates the formation of the homogeneous nanocrystals. When the temperature was increased during the reaction, the Se was first reduced to Se^{2-} ions and the Cu and In precursors decomposed. The reaction between the Se^{2-} and the Cu, and In ions initiates the nucleation of $CuInSe_2$.

Two possible nucleation mechanisms exist when the AAO template is employed. If the interactions between reagent molecules are stronger than those between the reagent molecules and the AAO pore walls, homogeneous nucleation near the pore centers would occur within the voluminous pores. Otherwise,

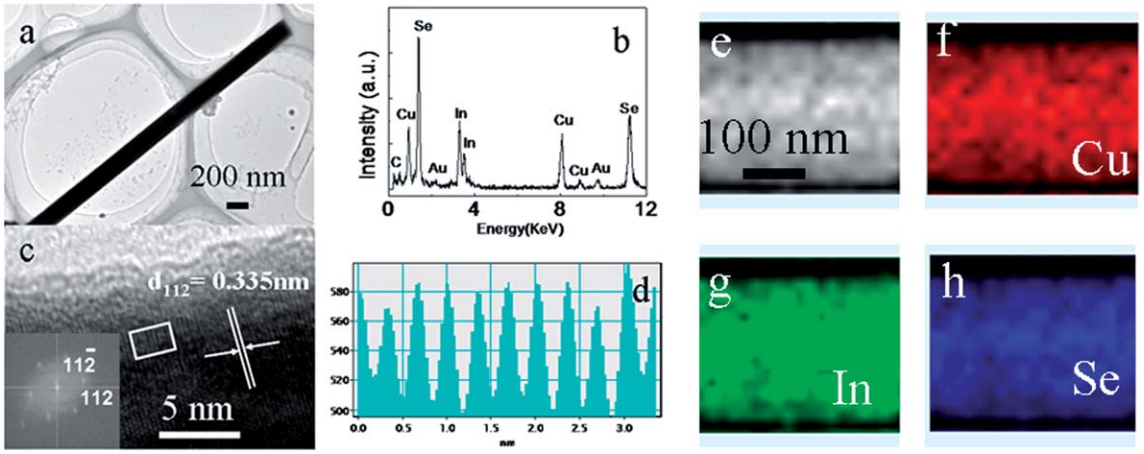

Fig. 5 TEM (a), HRTEM (c) images and EDX spectrum (b) of the as-prepared $CuInSe_2$ nanowires array. The inset of (c) shows a two-dimensional Fourier transform pattern of the lattice resolved image. (d) Line profile from the area marked with the rectangular frame in (c). (e) Dark-field TEM image of part of a $CuInSe_2$ nanowire; (f)–(h) the corresponding EDX elemental maps of Cu, In, Se.

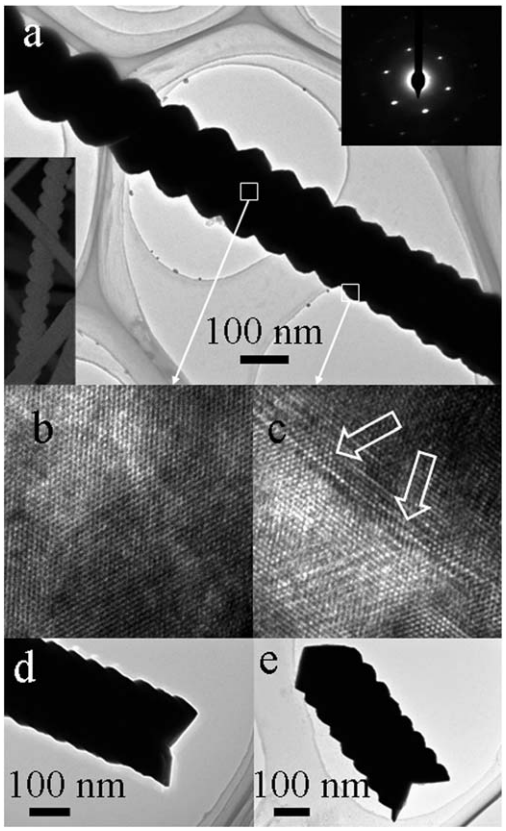

Fig. 6 (a) Typical TEM image of the as-prepared helical $CuInSe_2$ nanowires. Upper right inset: selected area electron diffraction pattern; lower left inset: typical SEM image of a $CuInSe_2$ helical nanowire. (b) HRTEM image of the helical $CuInSe_2$ nanowires showing clear lattice. (c) HRTEM image of the helical $CuInSe_2$ nanowires with some dislocations as shown with the arrows, (d) Cone shaped concave bottom of the helical nanowires. (e) Broken part of the helical nanowire with both the cone shape of the concave bottom and the protrusion tip.

heterogeneous nucleation would happen on the AAO pore walls. It has also been reported that heterogeneous nucleation on pore walls generally leads to polycrystalline materials in an AAO template-aided synthesis.[25] But our product is single crystalline nanowires. So, heterogeneous nucleation was not likely to have happened in the reaction. In addition, if heterogeneous nucleation takes the lead, one would expect the formation of $CuInSe_2$ nanotubes of short growth duration because crystal growth starts from the AAO pore wall. However, a time dependent growth discloses that a $CuInSe_2$ nanowire is always formed, and which is independent of the growth duration. This serves as another piece of supportive evidence for the homogeneous nucleation.

Once the homogeneous nucleation produced nuclei, the grain growth began. Considering the length scale of the nanowires and its single crystallinity over such a length scale, oriented attachment serves a possible mechanism due to its lack of involvement of diffusion of the grain boundary over large distance scales. An oriented attachment mechanism explains the crystal growth in which smaller particles with common crystallographic orientations directly combine together to form larger ones by crystallographic fusion at the planar interface. This mechanism is sometimes also called the grain-rotation-induced grain coalescence (GRIGC) mechanism[26,27] because the colliding random particles with no common crystallographic orientation tend to rotate into an orientation to obtain the structural accord at the interface. Then, a coherent grain–grain boundary is formed and disappears when a single larger nanocrystal is finally produced. Since our present crystal growth occurs in long confined AAO pores, oriented attachment with grain-rotation is more facilitated. In our present case, after the $CuInSe_2$ stable nuclei or grains with preferred orientation form near the centre of the pore, they attach and grow along the preferred growth axis [112] direction. During the nucleation process, the misoriented $CuInSe_2$ grains rotate or reorient along this [112] axis if sufficient volume is available to obtain the structural accord at the interface and induce further crystal growth.

However, in some cases, the $CuInSe_2$ grains are so large that insifficient space makes them rotate to obtain the complete structural accord at the interface and, as a result, the dislocation forms as shown in Fig. 6c. In this case, the screw dislocation driven crystal growth begins. The helical shape of the nanowires discloses that the atomic layers in the neighboring parts are not

parallel. The cone shape of the concave bottom and protrusion tip of the helical nanowires may result from the spiral growth step due to the screw dislocation. The helical shape of the nanowires and the cone shape of the concave bottom and protrusion tip provide direct evidence for the screw-dislocation-induced growth mechanism for the helical $CuInSe_2$ nanowires. Actually, screw-dislocation-driven growth has been successfully used to explain the formation of one-dimensional nanostructures including nanowires and nanotubes.[28–30] The new helical-type nanowires may induce the production of novel nanodevices and hence find their potential applications in the fields of nano-electronics, nanomechanics and nanosensors.

4. Conclusion

In conclusion, a simple solution approach has been developed for the fabrication of large scale $CuInSe_2$ nanowires arrays. During the reaction process, AAO was used as a morphology directing template and oleylamine acted as an activation agent. Two types of $CuInSe_2$ nanowires shapes were found to co-exist in the sample: one is straight nanowires, the other one is interesting helical nanowires. Growth mechanisms for the two types of $CuInSe_2$ nanowires arrays were also proposed based on the experimental results. An oriented attachment mechanism has been used to explain the growth of straight $CuInSe_2$ nanowires, while screw-dislocation-induced growth is believed to result in the formation of helical $CuInSe_2$ nanowires. UV-Vis optical properties showed that the bandgap of the as-prepared $CuInSe_2$ nanowires is 1.04 eV, disclosing their suitability for photovoltaic applications.

Acknowledgements

This work was supported by the National Natural Science Foundation of China (No. 21071135) and Q. Li acknowledges the funding from GRF under project No. 414908 and 414709.

References

1 S. H. Choi, E. G. Kim and T. Hyeon, *J. Am. Chem. Soc.*, 2006, **128**, 2520.
2 V. Nadenau, D. Braunger, D. Hariskos, M. Kaiser, C. Koble, M. Ruckh, R. Schaffer, D. Schmid, T. Walter, S. Zwergart and H. W. Schock, *Prog. Photogr. Res. Appl.*, 1995, **3**, 363.
3 J. Tang, S. Hinds, S. O. Kelley and E. H. Sargent, *Chem. Mater.*, 2008, **20**, 6906.
4 A. J. Wooten, D. J. Werder, D. J. Williams, J. L. Casson and J. A. Hollingsworth, *J. Am. Chem. Soc.*, 2009, **131**, 16177.
5 K. Ramanathan, M. A. Contreras, C. L. Perkins, S. Asher, F. S. Hasoon, J. Keane, D. Young, M. Romero, W. Metzger, R. Noufi, J. Ward and A. Duda, *Prog. Photovolt.*, 2003, **11**, 225.
6 D. T. Schoen, H. Peng and Y. Cui, *J. Am. Chem. Soc.*, 2009, **131**, 7973.
7 M. G. Panthani, V. Akhavan, B. Goodfellow, J. P. Schmidtke, L. Dunn, A. Dodabalapur, P. F. Barbara and B. A. Korgel, *J. Am. Chem. Soc.*, 2008, **130**, 16770.
8 Y. H. Yang and Y. T. Chen, *J. Phys. Chem. B*, 2006, **110**, 17370.
9 R. D. Schaller, M. Sykora, J. M. Pietryga and V. I. Klimov, *Nano Lett.*, 2006, **6**, 424.
10 L. Shi, C. J. Pei and Q. Li, *CrystEngComm*, 2010, **12**, 3882.
11 S. Phok, S. Rajaputra and V. P. Singh, *Nanotechnology*, 2007, **18**, 475601.
12 X. T. Zhang, Z. Liu, Q. Li, Y. P. Leung, K. M. Ip and S. K. Hark, *Adv. Mater.*, 2005, **17**, 1405.
13 H. Peng, D. T. Schoen, S. Meister, X. F. Zhang and Y. Cui, *J. Am. Chem. Soc.*, 2007, **129**, 34.
14 C. Persson and A. Zunger, *Phys. Rev. Lett.*, 2003, **91**, 266401.
15 W. B. Choi, B. H. Cheong, J. J. Kim, J. Chu and E. Bae, *Adv. Funct. Mater.*, 2003, **13**, 80.
16 O. Rabin, P. R. Herz, Y. M. Lin, A. I. Akinwande, S. B. Cronin and M. S. Dresselhaus, *Adv. Funct. Mater.*, 2003, **13**, 631.
17 T. A. Crowley, K. J. Ziegler, D. M. Lyons, D. Erts, H. Olin, M. A. Morris and J. D. Holmes, *Chem. Mater.*, 2003, **15**, 3518.
18 T. E. Mallouk, *Science*, 2001, **291**, 443.
19 Y. Mao and S. S. Wong, *J. Am. Chem. Soc.*, 2004, **126**, 15245.
20 H. Matsushita, S. Endo and T. Irie, *Jpn. J. Appl. Phys.*, 1992, **31**, 18.
21 J. P. Van der ziel, A. E. Meisner, H. M. Kasper and J. A. Ditzerberger, *Phys. Rev. B*, 1974, **9**, 4286.
22 J. L. Shay, B. Tell, H. M. Kasper and L. M. Schiavone, *Phys. Rev. B*, 1973, **7**, 4485.
23 C. M. Joseph and C. S. Menon, *J. Phys. D: Appl. Phys.*, 2001, **34**, 1143.
24 D. Pan, X. Wang, Z. H. Zhou, W. Chen, C. Xu and Y. Lu, *Chem. Mater.*, 2009, **21**, 2489.
25 M. E. T. Molares, V. Buschmann, D. Dobrev, R. Neumann, R. Scholtz, I. U. Schuchert and J. Vetter, *Adv. Mater.*, 2001, **13**, 62.
26 E. R. Leite, T. R. Giraldi, F. M. Pontes, E. Longo, A. Beltran and J. Andres, *Appl. Phys. Lett.*, 2003, **83**, 1566.
27 D. Moldovan, V. Yamakov, D. Wolf and S. R. Phillpot, *Phys. Rev. Lett.*, 2002, **89**, 206101.
28 S. A. Morin, M. J. Bierman, J. Tong and S. Jin, *Science*, 2010, **328**, 476.
29 M. J. Bierman, Y. K. A. Lau, A. V. Kvit, A. L. Schmitt and S. Jin, *Science*, 2008, **320**, 1060.
30 J. Zhu, H. L. Peng, A. F. Marshall, D. M. Barnett, W. D. Nix and Y. Cui, *Nat. Nanotechnol.*, 2008, **3**, 477.

